

# RFI MITIGATION IMPLEMENTATION FOR PULSAR RADIOASTRONOMY

*D. Ait-Allal<sup>1</sup>, R. Weber<sup>1,2</sup>, C. Dumez-Viou<sup>1</sup>, I. Cognard<sup>3</sup>, and G. Theureau<sup>1,3</sup>*

<sup>1</sup> Observatoire de Paris

Station de radioastronomie, F-18330 Nançay, France  
email: {dalal.ait\_allal, Cedric.Dumez-Viou}@obs-nancay.fr

<sup>2</sup> Institut PRISME, Université d'Orléans

Site Galilée, 12 rue de Blois, 45067 Orléans cedex 2, France  
email: Rodolphe.Weber@univ-orleans.fr

<sup>3</sup> Laboratoire de Physique et Chimie de l'Environnement et de l'Espace, UMR 6115 CNRS

F-45071 Orléans Cedex 02, France  
email: {icognard, theureau}@cnrs-orleans.fr

## ABSTRACT

The observation of known pulsars (pulsar timing) or the search for new pulsars can be limited by radio frequency interference (RFI) generated by Telecommunications activity. In this paper we propose several RFI mitigation techniques to cope with impulsive and/or narrow band RFI. For pulsar timing, we have implemented, a pulse blanker and a cyclostationary blanker, both in real time. For pulsar search, we propose a new approach which combines a hardware-efficient search method and some RFI mitigation capabilities. This method is based on a 2D FFT and Radon transform.

## 1. INTRODUCTION

Pulsars are rapidly rotating highly magnetized neutron stars which produce radio beams that sweep the sky like a lighthouse. The corresponding periodic pulse profiles can be measured with radio telescopes and dedicated backends. Figure 1 describes the typical steps of such a backend. If the pulsar is already known, radio astronomers are interested by its precise timing. A coherent de-dispersion processing is then implemented to compensate the frequency-dependent time-shift due to non-linearities in the interstellar medium (see [7] for more details). If not, an iterative search procedure is implemented to identify new pulsars.

In both cases, the quality of pulsar observations is limited by radio frequency interference (RFI) generated by various (and growing) Telecommunications activities. In this paper, we propose several RFI blanking techniques to cope with impulsive and/or narrow band RFI. Depending on where the detectors are implemented in the system, different types of RFI can be detected.

For pulsar timing, three possibilities have been identified on the system architecture defined on Figure 1:

- At the input of the polyphase filter bank, just after digitization. This configuration is appropriate for impulsive or burst broad-band RFI.
- Just after the polyphase filter bank.
- Just after the FFT. This configuration is more appropriate for narrow band and continuous RFI.

In sections 2 and 3, the implementation of two detectors is described. One is a Pulsed-RFI detection based on power criteria (case a), the other is a cyclostationary detector dedicated to continuous RFI (cases b and/or c).

For pulsar search, we propose a new approach which combines a hardware-efficient search method and some RFI mitigation capabilities both for impulsive and narrow band RFI. This method is based on a 2-dimensional FFT (2D FFT) and Radon transform. It covers case c. The algorithm is described in Section 4.

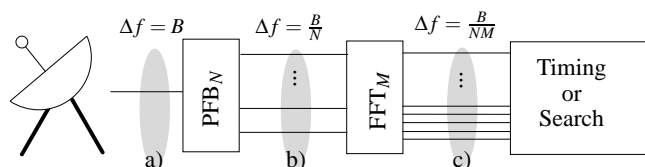


Figure 1: Typical pulsar backend architecture: a) step 1: waveform acquisition b) step 2: polyphase filter bank (PFB) to split the input frequency band (hundreds of MHz) c) step 3: During their travel through the interstellar medium, the pulsar pulses are progressively attenuated and spread over time. Time-frequency planes are calculated for real time de-dispersion procedure in the case of pulsar timing or for specific algorithm in the case of pulsar search (usually an off-line iterative search)

## 2. PULSED-RFI DETECTION WITH A POWER DETECTOR

In order to be efficient, the power detector needs a robust estimation of the decision threshold. Outlier samples that exceed this level are considered as interference and trigger the blanking of the corresponding data block before it enters the spectral estimation process. The problem is that the same block of data is used for threshold estimation and detection.

### 2.1 Threshold calculation

Uncorrupted complex data samples follow a normal distribution law since they result from the observation of a radio astronomical source more or less buried under system noise, both ideally following a Gaussian distribution. Thus, the instantaneous power of data samples follows a  $\chi^2$  distribution with two degrees of freedom.

Usually, power detectors are based on a Gaussian model. However, there are several disadvantages with such an approach. First, two parameters are needed to model the Gaussian distribution, mean and standard deviation. Furthermore, standard deviation estimation requires prior mean estimation. The error made on the mean estimate will affect the standard deviation estimate as well. Finally, in terms of logic resources and data bus width, the implementation cost of such an approach could be an issue (see Hampson [6]).

Our approach is based on the  $\chi^2$  distribution model. So, only one parameter (the mean  $\mu$ ) is needed to fully define the signal statistics. Consequently, the threshold value  $S$  is calculated as  $S = C\mu$  with  $C$  a parameter defined by the user. The mean value is recursively estimated (see Fig. 3-1). To make this estimation robust against outliers due to RFI, the strongest samples are system-

atically discarded. The effect of this clipping on mean estimation can be theoretically derived (Dumez-Viou [5]) and the proper correction is included in the parameter  $C$ . From this basic scheme, two improvements are proposed to enhance the performances for strong and weak radar pulses.

## 2.2 False alarm rate reduction

In detection systems, a given threshold defines a false alarm rate: samples that should not be classified as RFI trigger the detector because they lie in the right tail of the uncorrupted signal distribution, over the threshold value. This value has to be chosen such the false alarm rate is kept at a reasonably low level. Detecting weaker radar pulses can be achieved with a reduced threshold value leading automatically to an unacceptably rate of false alarm. Moreover, for synchronisation reasons, our detector blanks the whole block of data even if only one outlier has been detected in that block. This approach increases the false alarm rate. For example, if the threshold is set to  $4\mu$  to produce a 2.75% false alarm rate, a 2048-sample block configuration will systematically trigger the detector and the receiver returns no usable results.

To overcome this problem, note that the time distribution of such false alarms over the whole observation is uniform. Let  $\alpha$  be the false alarm rate. Then, the probability of obtaining  $N$  consecutive uncorrupted samples that trigger the detector is  $\alpha^N$ . Thus, triggering the blanker if three consecutive samples exceed the threshold sets a new false alarm rate of  $(2.75\%)^3 = 2.1 \times 10^{-3}\%$  leading to the blanking of only 6.4% of the data blocks.

The hardware required to handle the previous modifications is limited to a one-bit wide  $(N-1)$ -bit deep shift register to store the results of the comparisons between samples and threshold, and a  $N$ -bits AND gate. This approach ( $S = 4\mu$ ,  $N = 3$ ,  $\alpha = 2.75\%$ ) is used to detect strong radar pulses (see Fig. 3-2).

For weak radar pulses, considering  $N$  consecutive samples leads to poor detection performances, since radar bursts are increasingly buried under the system noise. However, tests have shown that counting the number of detections in a time window is better. Thus, for our weak pulse detector (see Fig. 3-3), we set the threshold to  $0.8125\mu$ , the time window to 30 samples and the triggering number of detection to 25. Using a binomial law and a tabulated  $\chi^2$  distribution, a false alarm rate of  $1.2 \times 10^{-3}\%$  is achieved, resulting in the blanking of 4% of the data blocks.

In terms of implementation, rather than adding the 30 bits for each new sample, we recursively calculate the sum. The balance (-1, 0 or +1) of '1' entering and '1' leaving the shift register is added to the previous count. The hardware now extends to a one-bit wide 30-bit deep shift register, a 1-bit subtractor and a 2-bit/5-bit adder.

Improving a basic power detector implies including some *a priori* knowledge. We focused on the pulse length, which is one of the basic characteristics shared by many radar systems. In this way, the detector is still generic but provides better performances for a slight increase in hardware costs.

The performances of our detectors are shown in Fig. 2. The blue curves annotated SP (respectively, WP) correspond to the behavior of the strong pulse detector (respectively, weak pulse detector). The results of two other previous studies have also been included in the figure. [9] are based on a simple pulse detector for two different settings (PP30 and PP90). [4] results are based on a much more advanced algorithm that gives better performances for its finest setting (AD05 and AD10). However, it includes a lot of information about a specific radar pulse shape. Any radar pulse whose shape differs significantly from the model will not be detected as easily.

## 2.3 Conclusion

The design operates at a maximum sampling rate of 145 Ms/s. The logic gates used to implement the algorithm occupy 4% of a 3 Mgates FPGA (Virtex II from Xilinx) and 2% of the 96  $18 \times 18$ -multipliers available. The design has been used to observe cosmic sources with flux densities as low as 5 mJy. No radar residuals could be seen on the base line as shown on figure 4.

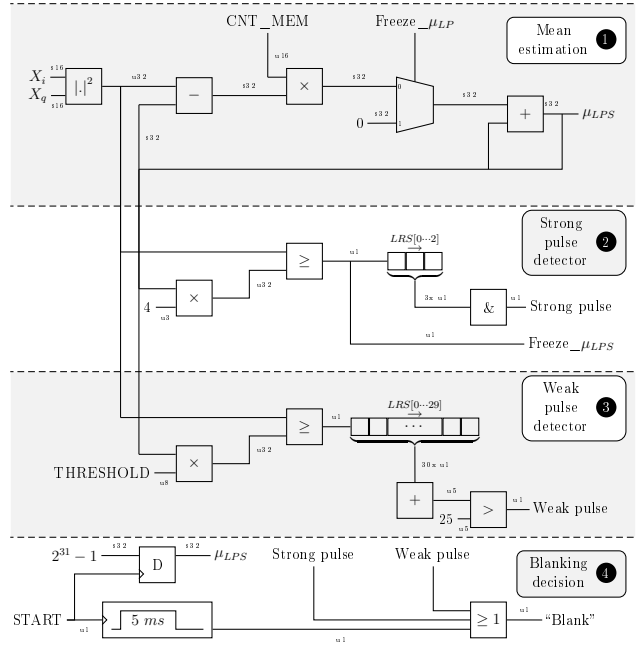


Figure 3: Hardware for the radar pulse blanker. LRS is a Logical Right Shift unit.  $s..$  and  $u..$  specify the databus widths for signed and unsigned operands.

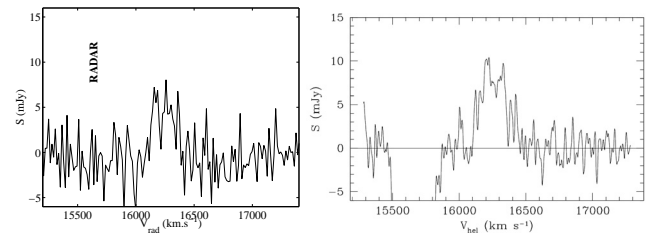


Figure 4: HI line of ESO 474-G26. Right: Observed at the Nançay Radio Telescope (NRT, [11]) with pulse blanking. left : Observed at NRT without pulse blanking.

## 3. CYCLODET: A CYCLIC DETECTOR

It is also possible to apply power detection on narrow band RFI. However, precise thresholding implies careful calibration of the frequency band and it assumes that the background power level of the signal is constant over time.

A better approach is to use a criterion that can differentiate quasi-steady noise-like signals from artificial or quickly varying signals. Cyclostationarity is such a criterion,[10]. Most telecommunication signals present a hidden periodicity due to the periodic characteristics involved in the signal construction (carrier frequency, baud rate, coding scheme...). These parameters are usually scrambled and hidden by the randomness of the message to be transmitted. In [1], we have demonstrated the interest of such an approach for pulsar applications. In the following, the detector principle is briefly presented and its real time implementation is described.

### 3.1 Principle of cyclostationary detection

We assume that  $x(t)$  is a mix of a stationary signal (*i.e.* a cosmic source and/or the system noise) and a cyclostationary signal (*i.e.* a RFI). Let us consider the following criterion:

$$C_N^\alpha = \frac{1}{N} \sum_{n=0}^{N-1} |x|^2(n) \exp(-j2\pi\alpha n) \quad (1)$$

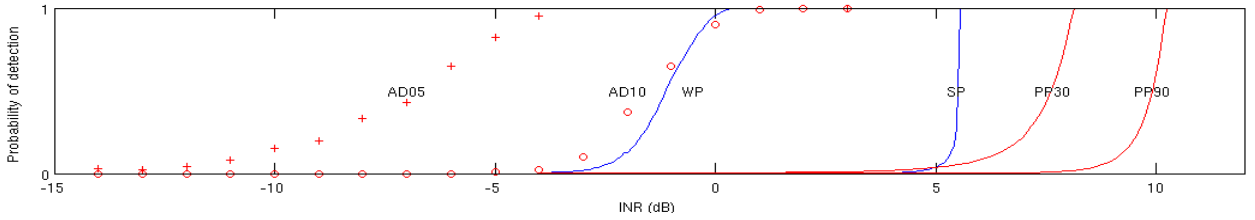


Figure 2: Probability of detection of several detectors as a function of radar pulse Interference to Noise Ratio (INR). AD05 and AD10 refer to [4]. PP30 and PP90 refer to [9]. WP and SP refer to the proposed hardware.

where  $\alpha$  is the cyclic frequency. This parameter is linked to the above-mentioned periodic characteristics. This detector expresses the search for periodicities in the instantaneous power fluctuations. To make this detector robust against slow power variations, we define a normalized version of our previous criterion:

$$D_N^\alpha = \frac{\sqrt{N}C_N^\alpha}{C_N^0} \quad (2)$$

In [12], we have derived the statistical properties of this detector as a function of the interference to noise ratio (INR).

### 3.2 Hardware implementation

From the above consideration, an operational cyclic detector has been implemented on a real time digital backend at Nançay Observatory. The algorithm is implemented into a digital programmable component Virtex II, an FPGA from the Xilinx company. The successive steps are (see also figure 5):

1. Channelization of the signal coming from the radio telescope. The signal in each channel is assumed to be complex. This process is done in real time by the digital receiver (*i.e.* output b or c in figure 1).
2. To reduce the computational load of the cyclic detector, the algorithm is applied to the real part only ( $s_r(n)$ ) of the signal. We compute the Fourier transform,  $FFT_N^m(f)$ , over  $N$  samples on  $s_r^2(n)$  for the  $m^{th}$  channel,  $m = 1, \dots, M$ .  $M$  is the number of channels.
3. According to a given threshold  $\xi$  derived from the theoretical study ([12]), we will consider that an RFI is present on the  $m^{th}$  channel if:

$$\exists k > 0 / \frac{\sqrt{N}|FFT_N^m(k)|}{FFT_N^m(0)} \geq \xi \quad (3)$$

with  $\xi = \sqrt{-2\log(p_{fa})}$

where  $p_{fa}$  is the expected probability of false alarm.

The design can process a 7 MHz frequency band. The logic gates used to implement the complex channelizer and the cyclic detector occupy 80% of the slices of a 3 M gates FPGA (Virtex II from Xilinx), 87% of the embedded memory and 88 of the 96  $18 \times 18$ -multipliers available. An external memory based on a SDRAM is also required to store a buffer of 2048x2048 16-bits complex-words (16 Mbytes).

Figure 6 shows some results obtained in the decameter band where calibration signals (wide band stationary noise) were used to simulate four pulsar pulses with different power levels. The red time-frequency slots correspond to RFI detected by our real time detector. Narrow band RFI are clearly detected. The detector is also sensitive to wide band RFI, and to noise diode power level transitions. The impulse or the step of power generated by these events produces a high frequency content in the cyclic spectra that triggers the cyclostationary detector. However, when the noise power

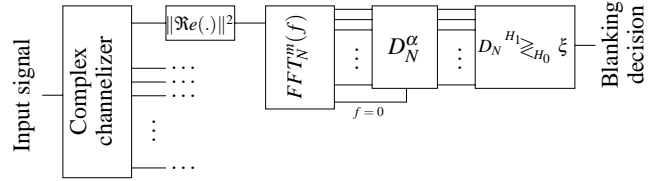


Figure 5: Cyclostationary detector algorithm

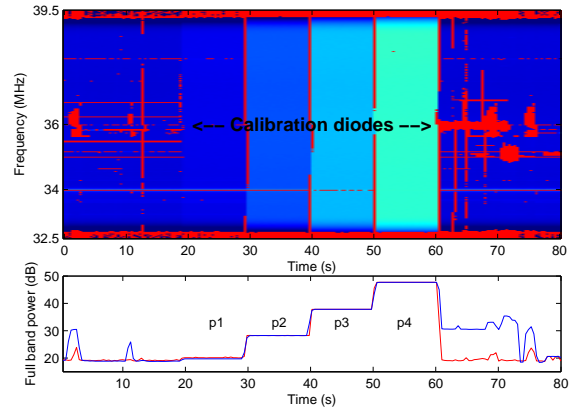


Figure 6: Results obtained in the decameter band at Nançay observatory. (top) Time-frequency power plane. The red time-frequency slots correspond to RFI detected by our real time detector. (bottom) Total power versus time. The red curve is the total power after blanking. The total bandwidth is 7 MHz. The number of channels is  $M = 2048$ . On each channel,  $N = 2048$  samples are used to compute the criterion. The cyclic detector is insensitive to steady power levels generated by the successive calibration noise diode pulses (p1 to p4) added to the signal.

returns to a steady state, the detector is again blind to power levels. For pulsar observations, these experiments demonstrated that the cyclostationary detector can discriminate between bursts due to pulsars and bursts due to RFI.

## 4. REAL TIME PULSAR SEARCH PROCEDURE

The search for new pulsars is a difficult task since neither the dispersion measure (DM) nor the periodicity are known. In figure 7.a, the classical search procedure is described. It consists in recording all the data and in trying off-line a set of DM and periodicities. This approach needs huge disk space and is quite time consuming. In this section, we propose a new real time pulsar search method, requiring less disk space, fewer computational resources and providing a simple way to blank RFI. It is based on a two dimensional Fourier

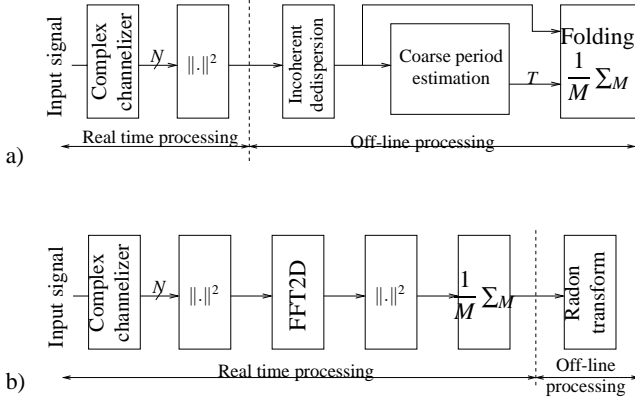


Figure 7: Different pulsar search procedures: (a) the classical approach. The output of the  $N$ -channel filter bank is stored. Off-line, different pulsar dispersion measures are used to de-disperse the pulsar pulses. Then, different periodicities are iteratively used to fold the successive pulsar pulses. (b) The 2D-FFT approach. A 2-dimensional FFT is applied on the output power of the  $N$ -channel filter bank providing an  $N \times N$  image. The average of  $M$  images are stored. Then, a Radon transform is applied.

transform (2D-FFT) and Radon transform. 2D-FFT is mentioned in the pulsar literature but only as a tool to search for periodicity ([2],[7] [8]).

#### 4.1 2D-FFT method

In figure 7.b, the different steps of the algorithm are presented and in figure 8 an example with a real pulsar pulse is provided for illustration. In short :

- The final output of the real time part consists of the  $N \times N$  image corresponding to the mean of  $M$  consecutive  $|2D - FTT|^2$  images. An example of such an image is given at figure 8.b. Each 2D-FFT is computed on independent  $N \times N$  time-frequency power planes such as the one provided at figure 8.a. With this approach, all dispersed pulsar pulses are projected at the same location in the 2D-FFT image. This location depends only on the pulsar DM and is different from the one obtained for RFI. In other words, any impulsive (respectively narrow band) RFI will be concentrated in the horizontal (respect. vertical) line centered in the 2D-FFT image. Thus, to remove RFI and to obtain a clean image, all that is required is to blank these vertical and horizontal lines which cross at the center of the 2D-FFT image.
- Off-line, a Radon transform is applied on the cleaned 2D-FFT image. It consists in summing the image intensity along successive radial lines [3]. When this integration line corresponds to the line where the pulsar pulses have been projected, all the pulsar power is concentrated in one point. At other integration angles, only the noise contribution will be integrated. Figures 8.c and 8.d illustrate this principle with respectively the dirty and clean image.

The advantage of this approach is that only a limited amount of data (the  $N \times N$  2D-FFT image) is stored for off-line processing. Furthermore, it provides simple RFI mitigation capabilities. In the following, we investigate the sensitivity of this approach compared with the classical one.

#### 4.2 sensitivity comparison

We consider the following signal model and algorithm parameters:

- The background noise is a white zero-mean Gaussian noise with power  $\sigma_n^2$ .
- The pulsar pulse is a white zero-mean Gaussian noise with power  $\sigma_p^2$ . The pulse duration is  $L$ . The signal to noise ra-

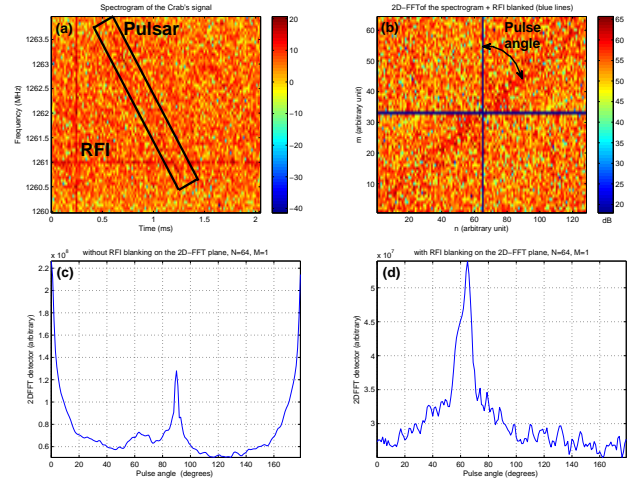


Figure 8: Application of 2D-FFT pulsar search approach on the Crab pulsar. (a)  $128 \times 64$  time-frequency power plane of the Crab pulse. We added a couple of synthetic RFI. (b) 2D-FFT image time-frequency power plane. The blue cross in the middle corresponds to the blanked RFI locations. (c) Radon transform of the dirty 2D-FFT image (*i.e.* RFI locations not blanked). The pulsar detection is not possible. (d) Radon transform of the clean 2D-FFT image. The pulsar can be easily detected.

tio is defined by  $SNR = \sigma_p^2 / \sigma_n^2$ . For the theoretical sensitivity derivation, we assumed that  $\sigma_p^2 \ll \sigma_n^2$ .

- There is no RFI.
- The t-f power plane dimension is  $N \times N$ .
- For the classical approach, we consider that the dispersion measure (DM) and the pulsar periodicity has been found by the ad-hoc iterative procedure. Thus, it is equivalent to assume 1) DM=0 (*i.e.* vertical pulse) and 2) pulses always occur at the same position in the t-f power plane. These t-f power planes are integrated over frequency to provide individual pulse profiles. Finally,  $M$  pulse profiles are summed together. The sensitivity,  $S_{classic}$  is defined by the average profile deviation due to the pulse over the noise only profile standard deviation.
- For the 2D-FFT approach, we set DM to zero as well. Indeed, with no loss of generality, we consider that zero-DM is just a DM among others. The central pixel of the 2D-FFT image is systematically blanked. The average of  $M$  2D-FFT planes provides the final clean 2D-FFT image. Finally, the Radon transform is applied for different angles. The sensitivity,  $S_{2DFFT}$  is defined by the Radon transform deviation at angle  $90^\circ$  over the Radon transform standard deviation at other angles.

This model is illustrated in figure 9. In particular, output examples of each approach are proposed and a graphical definition of sensitivity is provided. By considering the mean and the variance of this model at the successive algorithm stages, we have derived the following theoretical equations:

- for the classical case:  $S_{classic} = \frac{\sigma_p^2}{\sigma_n^2 / \sqrt{NM}} = SNR \sqrt{NM}$
- for the 2D-FFT case:  $S_{2DFFT} = \frac{T \sigma_p^4}{\sigma_n^4 / \sqrt{NM}} = T \cdot SNR^2 \sqrt{NM}$  where  $T = L/N$  (*i.e.*  $T$  is pulse width in the t-f power plane).

In figure 10, these sensitivities have been computed by simulation for different parameters. Theoretical sensitivity are also plotted. From this figure, several remarks can be stated:

- It is shown that theory and simulations fit together. The shift for ( $SNR = 0$  dB,  $L = 2048$ ) is due to the fact that our assumption ( $\sigma_p^2 \ll \sigma_n^2$ ) is no longer valid.
- The 2D-FFT sensitivity is proportional to  $SNR^2$ . This makes

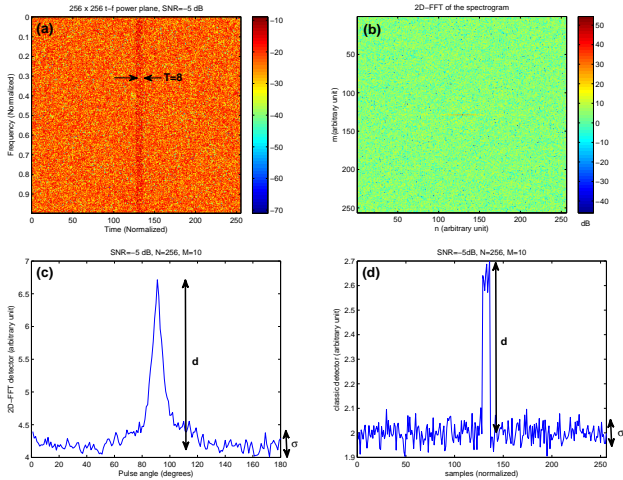


Figure 9: Application of the classical and 2D-FFT pulsar search approach on our zero-DM model. (a) Time-frequency (t-f) plane ( $N = 256$ ) of one pulsar pulse with  $\text{SNR} = -5$  dB,  $L = 2048$ ,  $N = 256$  and  $T = L/N = 8$ . (b) Average 2D-FFT image of  $M = 10$  t-f planes. (c) Output of the Radon transform. The peak position is directly related to the DM. Here  $DM = 0 \Rightarrow \text{angle} = 90^\circ$ . (d). Output of the classic approach. For both cases, the sensitivity is defined by the ratio  $d/\sigma$ .

this approach less sensitive to low SNR compared with the classical approach (see for example the case ( $\text{SNR} = -5$  dB,  $L = 256$ )). This drawback is counterbalanced by the fact that the 2D-FFT approach is also sensitive to the pulse width,  $T$ . The wider the pulse is, the better the 2D-FFT detection is (see case ( $\text{SNR} = -5$  dB,  $L = 2048$ )). In some cases, the 2D-FFT approach can outperform the classic method (see case ( $\text{SNR} = 0$  dB,  $L = 2048$ )).

- These detection performances are achieved without knowing anything about the pulsar (neither the DM nor the periodicity). This is not the case for the classical pulsar search procedure, where the derived performances are only achieved when exact DM and periodicity are known.

The next step will be to test the algorithm with different configurations of real pulsar data and real RFI.

## 5. CONCLUSION

Several RFI mitigation techniques applicable to pulsar observation have been presented. In the case of pulsar timing, a Pulsed-RFI detector and a cyclostationary detector have been implemented for real time experiments. In the framework of the UNIBOARD FP7 European project, these algorithms will be implemented in a multi-purpose scalable computing platform for Radio Astronomy as part of the pulsar receiver. In the case of pulsar search, a new approach which combines a hardware-efficient search method and some RFI mitigation capabilities has been proposed. It could be an alternative for the next generation of radio telescopes such as the LOFAR radio telescope ([www.lofar.org](http://www.lofar.org)) or the Square Kilometer Array (SKA, [www.skatelescope.org](http://www.skatelescope.org)) where the huge amount of data to be processed by classical search procedures is an issue.

*Acknowledgements.* The authors would like to thank the European Commission Framework Program 7 (Project PrepSKA (contract no 212243) and Project Radionet/Uniboard (contract no 227290)), The French funding agency ANR (contract ANR-09-BLAN-0225-04) for funding part of this work.

## REFERENCES

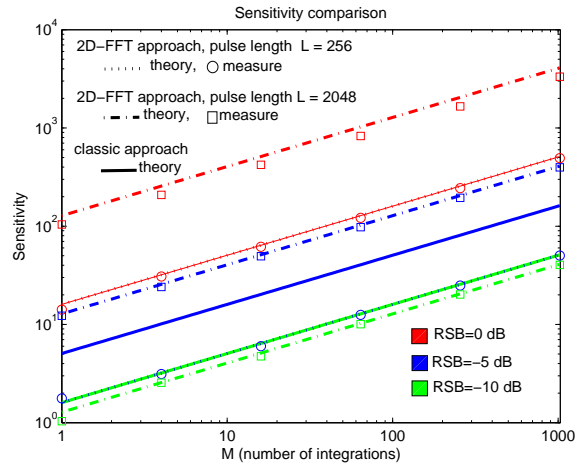


Figure 10: Comparison of the 2D-FFT and the classic pulsar search procedures ( $N = 256$ ). 3 SNR (0 dB,  $-5$  dB and  $-10$  dB) and 2 pulse lengths ( $L = 256$  and  $L = 2048$ ) have been simulated for different values of  $M$ . The continuous and dashed curves correspond to theoretical values. Box and circles correspond to 2D-FFT sensitivity measurements through simulations.

- [1] D. Ait-Allal, R. Weber, I. Cognard, G. Desvignes and G. Theureau, "Rfi mitigation in the context of pulsar coherent de-dispersion at the Nançay radio astronomical observatory" in *Proc. EUSIPCO 2009*, Glasgow, UK, September 4-8, 2009.
- [2] F. Camilo, D.J. Nice, J.A. Shrauner, and J.H. Taylor, "Princeton-Arecibo Declination-Strip Survey for Millisecond Pulsars. I.," *The Astrophysical Journal*, vol. 469, 1996, pp. 819-827.
- [3] S. Deans, "The radon transform and some of its applications" Krieger Pub. Co., 1983
- [4] W. Dong, B.D. Jeffs and J.R. Fisher, "Kalman Tracking and Bayesian Detection for Radar RFI Blanking," RFI2004, Workshop in Mitigation of Radio Frequency Interference in Radio Astronomy, Penticton, Canada, July 2004
- [5] C. Dumez-Viou, "Radioastronomical sources restoration from hostile radioelectric environment: Implementation of real-time detectors for dynamic spectra analysis," PhD thesis, <http://tel.archives-ouvertes.fr/tel-00319939/fr/>, September 2007
- [6] G.A. Hampson, "Implementation of the Asynchronous Pulse Blanker," June 2002. <http://esl.eng.ohio-state.edu/~rstheory/iip/docserv.html>
- [7] D. Lorimer and M. Kramer "Handbook of pulsar astronomy," Cambridge (GB): Cambridge University Press, 2005.
- [8] A. Lyne and F. Graham-Smith "Pulsar astronomy," Cambridge: Cambridge University Press, 2006.
- [9] N. Niamsuwan, J.T. Johnson and S.W. Ellingson, "Examination of a simple pulse-blanking technique for radio frequency interference mitigation," *RADIO SCIENCE*, 40(3), June 2005
- [10] E. Serpedin, F. Panduru, I. Sari, and G.B. Giannakis, "Bibliography on cyclostationarity" *Signal Processing*, vol. 85, pp. 2233-2303, Dec. 2005.
- [11] Station de radioastronomie de Nançay, France, [www.obs-nancay.fr](http://www.obs-nancay.fr)
- [12] R. Weber, P. Zarka, V. Ryabov, R. Feliachi, J. Grießmeier, L. Denis, V. Kozhyn, V. Vinogradov, and P. Ravier, "Data preprocessing for decametre wavelength exoplanet detection: an example of cyclostationary rfi detector," *Eusipco*, Poznan, Poland, 2007.